

Landslides (2022) 19:451–463  
 DOI 10.1007/s10346-021-01840-0  
 Received: 15 October 2021  
 Accepted: 25 December 2021  
 Published online: 7 January 2022  
 © Springer-Verlag GmbH Germany,  
 part of Springer Nature 2022

Hasnain Gardezi · Aiguo Xing · Muhammad Bilal · Yu Zhuang ·  
 Shoaib Muhammad · Shahmir Janjua



## Preliminary investigation and dynamic analysis of a multiphase ice-rock avalanche on July 5, 2021, in the upper Naltar valley, Gilgit, Pakistan

**Abstract** On July 5, 2021, a catastrophic rock avalanche hit an area in the upper Naltar valley, located in northwestern Gilgit, Pakistan. The 14 Mm<sup>3</sup> rock mass flowed down the hillslope and traveled a distance of approximately 5 km. The avalanche killed four people and damaged more than 150 livestock. Based on a field investigation, the event is classified as a dual-phase avalanche comprising glacial ice and rock mass mixtures. In this study, the runout behavior and characteristics of the upper Naltar rock avalanche are analyzed using DAN3D. The simulation results indicate that the propagation process lasted for 140 s, with an average maximum velocity of 32 m/s. The frictional-Voellmy model for the materials in the source and erosion areas produced the best results for DAN3D. Parameter calibration, model performance, and verification were performed numerically and based on field observations. It is hoped that the selected model and parameters will help the relevant agencies understand the propagation process of similar kinds of rock avalanches in the area surrounding the current avalanche, thus improving the hazard zonation in this region.

**Keywords** Ice-rock avalanche · Propagation modeling · High-speed long-runout · Upper Naltar valley Pakistan

### Introduction

Northern areas in Pakistan are experiencing an increase in atmospheric temperature, resulting in enhanced glacial melting, glacial lakes, and snow and ice avalanches (Negi et al. 2018; Kumar et al. 2019; Pandey et al. 2021a). Snow and ice avalanches can cause multiphase events that can achieve high speeds and cause disastrous effects downstream (Runqiu 2009; Chigira et al. 2010; Xu et al. 2014) by entraining large volumes of rock and slope material and forming dammed lakes (Mergili et al. 2018). Two-phase landslides, such as ice-rock debris avalanches, are more dangerous than ordinary debris flows, as they can be highly mobile and have long runouts. In recent years, these ice-rock mix avalanches have caused disastrous effects on population and infrastructure (Gnyawali et al. 2020; Shugar et al. 2021).

These climatic variations in high mountain ranges may cause the weakening of glacial permafrost linkages by cyclic freeze and thaw, which can result in slope failure (Fischer et al. 2013; Pandey et al. 2021b). The latest multiphase rock avalanche occurred in the upper Naltar valley on July 5, 2021, when 14Mm<sup>3</sup> of rock mass and glacial ice flowed down the hill slope and covered a runout distance of 4480 m. Small landslides with a short runout can be prevented with typical civil engineering measures, but high-speed long-runout landslides and avalanches can be avoided only by taking adequate

preventive and mitigation measures such as early warning systems and evacuation from vulnerable areas (Kilburn and Petley, 2003; Xing et al. 2016). The prediction of landslide characteristics such as runout distance, velocity, energy, and volume can be of great importance for risk assessment in landslide-prone areas. Many numerical studies and modeling techniques have been performed to better understand these events (Hutter et al. 1995; Campbell et al. 1995; Hungr and Evans, 2004; Hungr and McDougall, 2009; Scheidl et al. 2013; Revellino et al. 2013; Guerriero et al. 2014; Abe and Konagai, 2016; Zhuang et al. 2019; Abraham et al. 2020). In many cases, back analysis has been a suitable method to establish parameters for the future forecasting of similar kinds of events in such areas.

In the recent past, numerous techniques have been used to analyze landslides, such as discontinuous deformation analysis (DDA), the three-dimensional numerical modeling code (3DEC), the particle flow code (PFC), and discrete element modeling (DEM) (Crosta et al. 2003; Zhang et al. 2015; Wu et al. 2017; Chen and Wu, 2018). Several researchers have also used finite element modeling (FEM) and smoothed particle hydrodynamics (SPH) techniques to analyze landslides (Chen et al. 2007; Ishii et al. 2012; Leshchinsky et al. 2015; Chen et al. 2019; Pradhan and Siddique, 2020; Ma et al. 2021; Huang et al. 2012; Pastor et al. 2014; Zhu et al. 2018; Wang et al. 2019; Lin et al. 2019).

The present study uses a meshfree method, namely, the three-dimensional dynamic analysis DAN3D, to analyze and determine the characteristics of the upper Naltar valley avalanche. DAN3D is based on the S.P.H. method, has and shown accurate performance in analyzing long-runout landslides (McDougall and Hungr 2004). It also allows to consider the entrainment effect and considers the mass as equivalent flow. DAN3D has been widely used to analyze many North American and South Italian landslides, whereas in Pakistan, the model has been used to accurately determine the Attabad landslide characteristics (Gardezi et al. 2021). The study determines the runout behavior and dynamics of the upper Naltar valley avalanche on the basis of thorough field investigation and numerical modeling. The outcomes of this study will help the relevant agencies in disaster prevention and mitigation in this area.

### Description of the study area

The upper Naltar valley ice-rock avalanche is located in the Gilgit district, a tourist attraction located approximately 60 km northwest of Gilgit, Pakistan. The valley is situated in the Karakoram Mountain range, and its orientation is strongly controlled by the area's tectonics. The Naltar valley is controlled by two main thrusts: the Main Karakoram Thrust (MKT) and Main Mantle Thrust (MMT).

The MKT is on the northern end and is also known as the northern mega shear, which represents the southern part of the Eurasian plate in Asia. It is a steeply dipping and seismically active thrust and has accounted for most of the earthquakes in the study area (McDougall et al. 1993). The MMT, also known as the southern mega shear, is a north-dipping thrust that separates the Indian plate from the Kohistan arc, as shown in Fig. 1. Rocks in the area are highly weathered and can be characterized as part of the Kohistan arc, which is composed of igneous intrusions, i.e., the Kohistan batholith. The entire region, especially the area around the landslide site, is deeply bisected by streams fed by melting glacial ice and snow. Landslides are frequent in the upper Naltar valley, and thus far, seven lakes have been formed due to the blockages caused by landslides such as debris flows, rockfalls, and avalanches.

Methodology

Field investigation

A detailed field investigation of the upper Naltar valley rock avalanche was carried out on August 25–27, 2021. The field measurements including landslide boundary, superelevation angle, deposit thickness, boulder size, and slope were carried out using a total station with and without the help of a prism. Two local residents were hired to carry the prism to difficult locations, i.e., the source area of the avalanche. The deposit thickness on both branches was

measured using the total station. The instrument was fixed on a high location, and measurements were taken by moving the prism around the deposit area. Measurements near the station were taken without a prism, whereas long-distance measurements were taken with the help of a prism. Based on the deposit thickness measurements on both branches, the total avalanche volume was estimated.

Rock samples were also collected for the petrographic study. Aggregate samples collected from the landslide area were thoroughly washed to remove the dust and dried in the laboratory. A hand lens was used to observe the grain sizes and colors of the representative pieces. Thin sections (petrographic sections) were prepared from the samples and studied under a petrographic microscope using both cross-polarized and plane light under low and high magnification.

Numerical runout modeling of the upper Naltar valley avalanche

To investigate the dynamic characteristics of the upper Naltar valley avalanche, the DAN3D dynamic model proposed by McDougall and Hungr (2004) was used. The model is based upon a numerical solution of the depth-averaged shallow water equation, and further, it has been modified for landslide simulations. The model is governed by the basal friction angle and internal rheological properties. There are five rheological models in DAN3D, among which the combination of the frictional and Voellmy models have shown

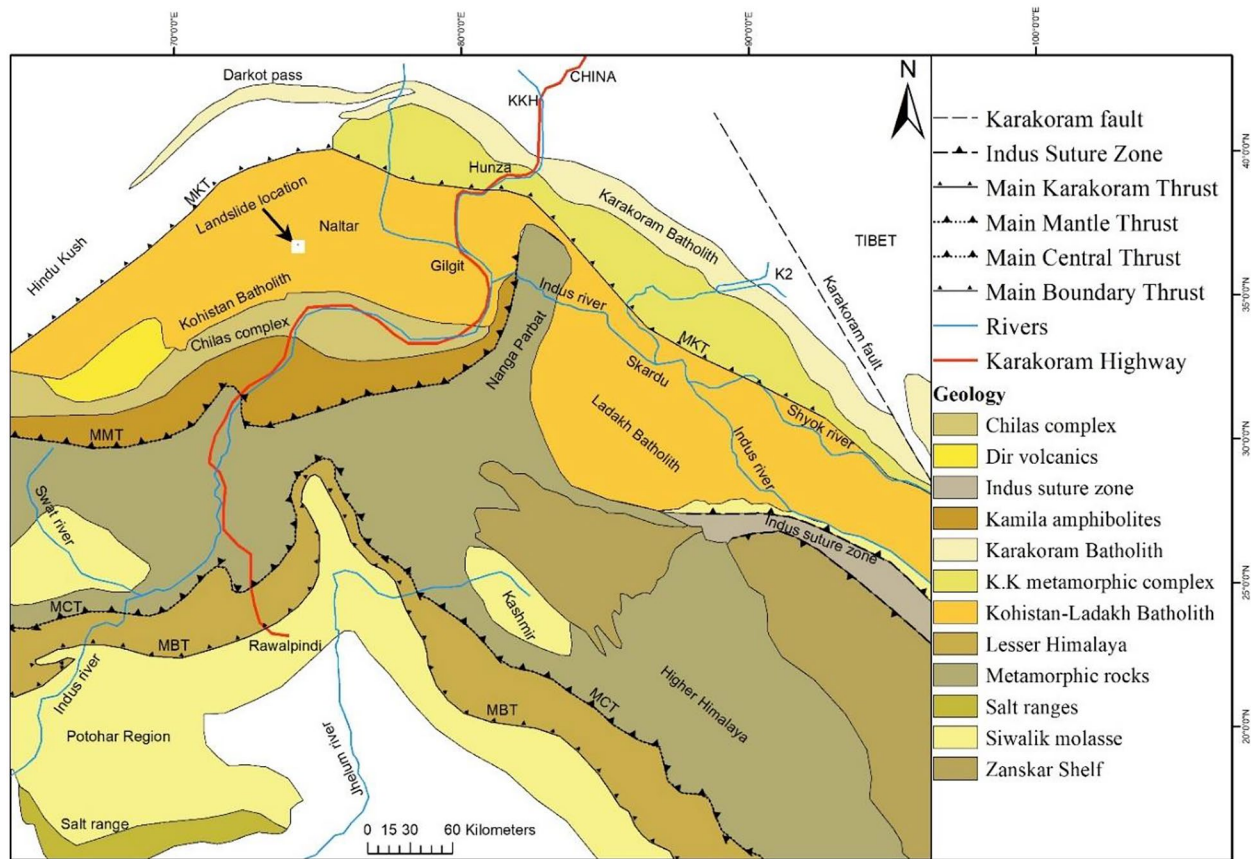


Fig. 1 Geological map of the study area

the most accurate results while simulating case studies (Xing et al. 2017; Zhuang et al. 2019; Aaron et al. 2020; Gardezi et al. 2021). The frictional model that governs the landslide source area represents the basal resistance as a function of effective normal stress ( $\sigma$ ) acting on the sliding surface. It can be represented as follows:

$$\tau = \sigma(1 - r_u) \tan \varphi \quad (1)$$

where  $\sigma$  represents the effective normal stress,  $u$  represents the pore water pressure,  $r_u$  is the ratio between the pore water pressure and total normal stress acting at the base of the sliding material, and  $\varphi$  is the dynamic friction angle. The relation between the dynamic friction angle and pore pressure can be represented by a single basal friction angle  $\varphi_b$ .

$$\sigma_b = \arctan(1 - r_u) \tan \varphi \quad (2)$$

The Voellmy model, which was used in the entrainment area, considers total resistance, which is composed of frictional and turbulent parameters and can be represented as follows:

$$\tau = \sigma f + \rho g v^2 / \varepsilon \quad (3)$$

where  $f$  represents the friction coefficient that relates shear stress to normal stress,  $\rho$  is the density of the sliding material in  $\text{g/cm}^3$ ,  $g$  is the gravitational acceleration,  $v$  (m/s) is the velocity of the sliding material, and  $\varepsilon$  ( $\text{m/s}^2$ ) is the turbulency coefficient. Initially, the sliding mass is moved as a solid block, and later, during downward movement, it disintegrates and behaves as a fluid.

The detailed rheological parameters of the upper Naltar valley avalanche for DAN3D are indicated in Table 1. The properties, such as the density of the sliding material, were determined by collecting samples from the field and testing them in the lab. The rheological parameters were determined by the hit and trial method until the results were consistent with in situ conditions (runout distance, volume, and travel path). The volume of the sliding mass was significantly increased during movement through the entrainment area. According to McDougall and Hungr (2004), the average erosion rate  $E_s$  for the landslide can be obtained by using the following equation:

$$V_f = V_0 \exp(E_s S) \quad (4)$$

where  $V_f$  indicates the estimated final volume of the sliding mass in  $\text{m}^3$ ,  $V_0$  is the initial volume in  $\text{m}^3$ , and  $S$  represents the runout length. The volume growth rate according to Eq. 4 was found to be  $2.29 \times 10^{-4} \text{ m}^{-1}$ .

In the present study, we used the frictional and Voellmy models for the materials located in the source and erosion areas, respectively. To accurately simulate the landslide, the basal rheological parameters were adjusted by the hit and trial method such that the output results were consistent with in situ conditions (McDougall

et al. 2006; Sosio et al. 2008; Revellino et al. 2013; Guerriero et al. 2014; Wu et al. 2015; Yin et al. 2017). While simulating the landslide, the Voellmy parameters were well in the range of the values and were found to be suitable for most of the case histories with long runouts. The simulations revealed that the runout distance is highly sensitive to the coefficient of friction, dynamic friction angle, and turbulence coefficient. As the friction coefficient and dynamic friction angle increase, the landslide runout distance decreases, and vice versa. However, the increase in the turbulence coefficient increases the runout distance of the landslide for the same friction coefficient values.

The digital elevation model used in DAN3D for the propagation modeling of the upper Naltar valley rock avalanche was obtained using the Shuttle Radar Topography Mission (SRTM) 1 arc-second. Whereas the  $28 \times 28$  m post-event DEM was obtained from a local disaster management agency, the pre-event  $30 \times 30$  m DEM was resampled at  $28 \times 28$  m using the kriging method in ArcMap and a DEM of difference was prepared by subtracting post-event DEM from pre-event DEM. The results obtained from propagation modeling were validated by comparing them with field investigation. Furthermore, the usefulness of the DAN3D module to estimate the velocity of the present study can be verified by comparing the results with a simple equation of motion.

$$S = Vt \quad (5)$$

where  $S$  is the distance (m),  $V$  is the velocity (m/s), and  $t$  indicates the time in seconds, while Eq. 6 (Evans et al. 2001) was used to validate the superelevation velocity obtained from numerical simulations.

$$V = (gd r/b)^{1/2} \quad (6)$$

>where  $d$  is the superelevation (m),  $r$  is the radius of curvature, and  $b$  is the width of the runout path. The measurements for  $d$ ,  $r$ , and  $b$  were also taken with the help of the total station.

## Results and discussions

### Landslide characteristics

On July 5, 2021, at 09:30 am Pakistan Standard Time (PST), a mixed ice-rock avalanche occurred in the upper Naltar valley. According to the report by the National Disaster Management Authority (N.D.M.A.) of Pakistan, four people lost their lives, and many livestock and nearby structures were destroyed in the avalanche.

The multiphase rock avalanche was initiated at an elevation of 5000 m. Figure 2a represents the areal image of the avalanche location. The avalanche traveled a total distance of 4480 m with an elevation difference of 1830 m and covered an area of  $1.7 \text{ km}^2$ . The final volume of the landslide was  $14 \text{ Mm}^3$ . The source area is at an elevation of 5000 m, while the toe is at 4480 m above mean sea level. The average length and width of the source area are 520 m and 400 m, respectively. According to the field observations, the avalanche, after detaching from the source area, traveled through a predefined path, a gully formed between two mountains. The avalanche entrained material from a vast area between 4480 and 3300 m in elevation and has an approximate length of 2780 m. At the same time, the elevation of the deposit area varies from 3300 to 3170 m. Based on the field investigation, the engineering geological

**Table 1** Selected models and back-calculated values for rheological parameters

Area	Rheology type	$\varphi^\circ$	$r_u$	$f$	$\xi(\text{m/s}^2)$
Source area	Frictional	45°	0.02	-	-
Erosion area	Voellmy	-	-	0.05	400

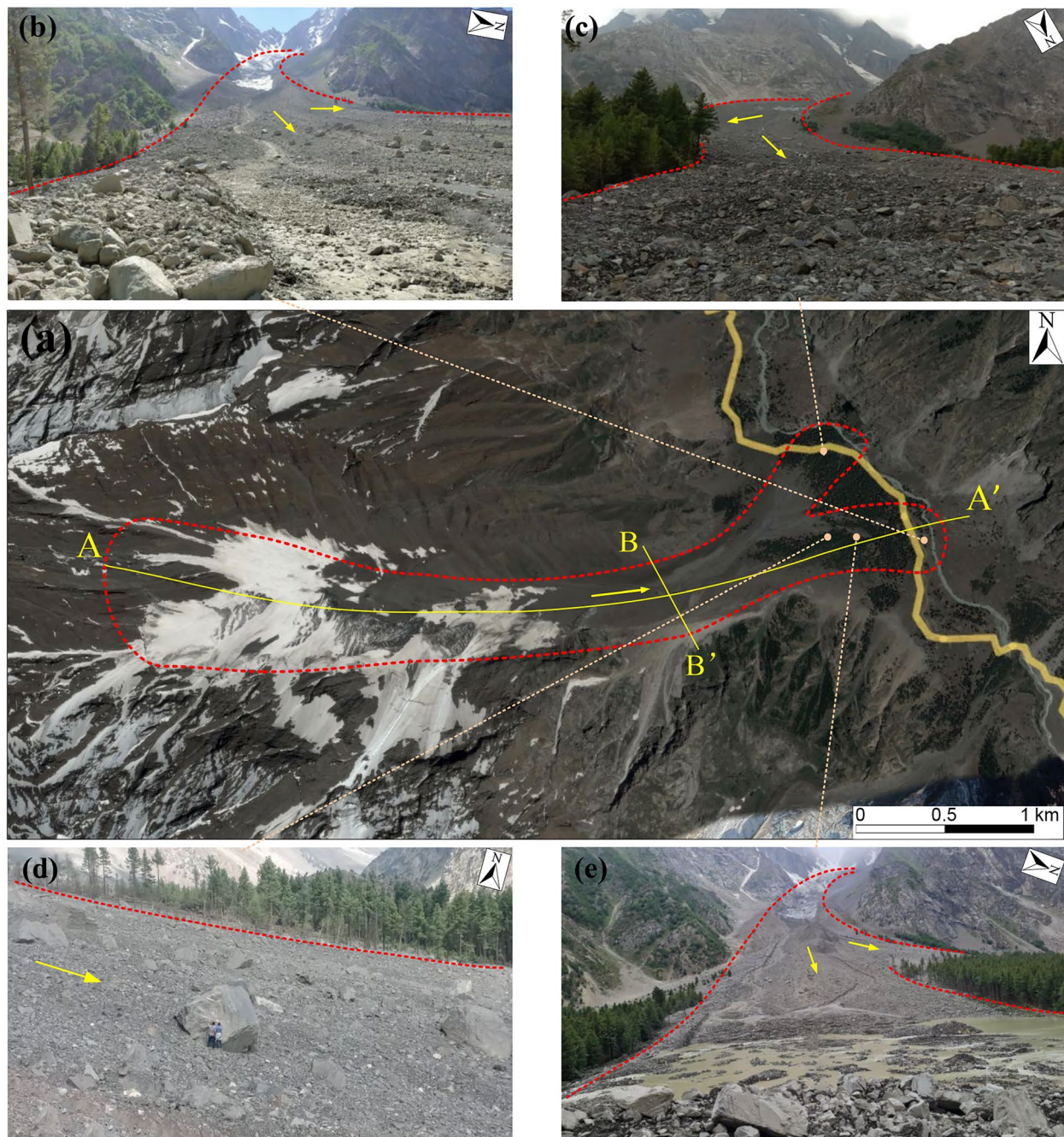


**Fig. 2** (a) Pre-landslide images of the deposit area. (b) Material deposited on the straight branch. (c) Material deposited on the left branch. (d) Massive boulders scattered on the straight branch. (e) Melted glacial ice in the deposit area

cross-section along line A-A' of the upper Naltar avalanche is presented in Fig. 3.

The sliding material was a mixture of sizeable glacial ice chunks and rocks of different sizes. Two major types of rocks were found in the landslide deposit area during the field investigation: granodiorite and andesite. The petrographic analysis shows that andesite rocks contain 52% chloridized-amphibole, while the major component of granodiorite is quartz at 46%. The results also indicate that feldspar is the second major component in both samples; however,

the proportion is higher in granodiorite, approximately 40 compared to 29% in andesite. The results are presented in Table 2. Figures 2b and 2c show the deposition of material along the straight and left branches. The deposit area is composed of rocks varying in size from cobbles to massive boulders, some having diameters between 17 and 20 m, and some are scattered across the deposit area, as shown in Fig. 2d. The average size ranges between 1 and 3 m. The glacial ice mixed with the rock mass melted soon after accumulating in the deposit area; as shown, Fig. 2e shows that the glacial ice

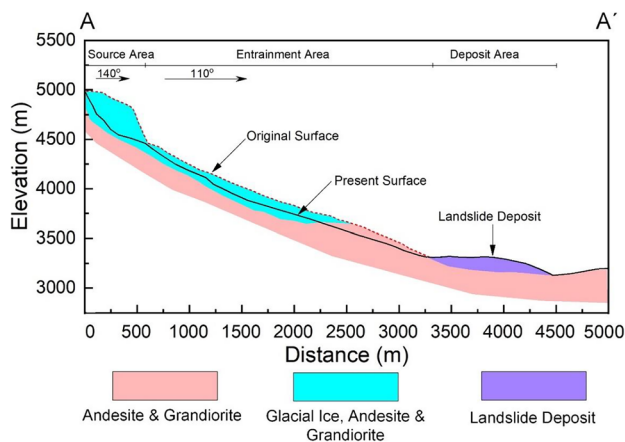


**Fig. 3** Longitudinal profile of upper Naltar valley avalanche along the section A-A'

chunks mixed with the rock mass melted soon after accumulating in the deposit area, leaving behind the rock mass. One of the local residents, who was driving a jeep near the landslide site, captured a video of the avalanche when it entered the valley; images taken from the video footage are shown in Fig. 4.

Considering field observations, after dethatching from the source area, the avalanche rapidly moved downhill in the S-E direction. At an approximate distance of 1500 m from the source area, the entire runout path is tilted by 30°, and the ice-rock mix avalanche traveled along that bend and continued to move toward the valley. At an elevation of 3560 m above sea level (a.s.l.), the avalanche superelevated and turned, as shown along line B-B' in Fig. 2a. Figure 5 shows the

superelevation along the runout path, while Fig. 5a presents the site conditions of the gully. Figure 5b shows the angle of superelevation and Fig. 5c presents the sectional profile along line B-B'.

The fluidized landslide was divided into two branches at the valley threshold. Figure 6a shows the location of the superelevation and both branches of the avalanche, while Fig. 6b presents the abrasion along the valley slopes caused by the movement of the avalanche. Both branches separated at an angle of 54°; one branch traveled straight along the runout path, while the second branch deflected in a N-E direction. The straight branch has an average width of 350 m, while the left branch is approximately 300 m wide. The deposit material thicknesses in the straight and left branches are approximately 23 m and 19 m, respectively. These two branches blocked the valley at two points that interrupted stream flow. The blockage of the stream at two locations led to the temporary formation of two dammed lakes. Two days after the landslide occurred, the left branch was overtopped by the water accumulated behind it, thus forming a larger lake. The dammed lake and subsequently dried stream are shown in Figs. 7a and 7b.

### Landslide propagation

The volume of the avalanche was calculated from the difference in the DEM and found to be approximately 14 Mm<sup>3</sup>. The DEM of the differences is shown in Fig. 8. The validation process was carried out by comparing the results of propagation modeling, field investigation, and equations. According to the results obtained from DAN3D, the avalanche had a total runout distance of 4550 m and a runout duration of 140 s. The predicted final deposit distribution of the upper Naltar valley avalanche is displayed in Fig. 9. Figure 10 indicates the depth at different time steps, i.e., 10 s, 30 s, 50 s, 70 s,

**Table 2** Petrographic study of andesite and granodiorite rocks

Sample	Components	Percentage (%)	Description
Andeiste	Chloritized-amphibole	52	It occurs as altered amphibole as a result of chloritization
	Feldspar	29	Plagioclase diagnostic twinning is occasionally observed, as the feldspars show alteration
	Quartz	11	It occurs as subhedral grains with wavy extinction as a result of the deformed nature
	Epidote	5	Present in small proportion and alters the pyroxene after epidotization
	Pyroxene	2	Present in a minimal amount in an altered state due to epidotization
	Ores	1	Very minute proportion and the ore exists as a single grain of subhedral to irregular pyrite and magnetite
Granodiorite	Quartz	46	The quartz grains are highly strained with a size ranging between 0.5 and 1.7 mm
	Feldspar	40	It is primarily composed of plagioclase having a size range the same as the quartz grains and shows partial alteration to sericite and clay. Also, despite alteration, the plagioclase shows diagnostic twinning
	Biotite	10	It exists in a cluster form or discrete grains and shows alteration to ores
	Amphibole	4	Present in a small percentage, and show alteration to chlorite
	Ores	2	Present in minute proportion

**Fig. 4** Still image from the video footage showing the landslide runout through the valley



90 s, 110 s, 130 s, and 140 s. The simulation results show a deposit depth of less than 5 m near the toe of the slide on both branches, while a maximum thickness of 25 m was observed on the straight branch and a maximum thickness of 20 m was observed on the left branch of the deposit area, which is consistent with the field observation data, i.e., 23 m and 19 m, respectively.

Furthermore, the slide accumulated a considerable amount of material from the entrainment area, which is evident from the simulation results. The  $7.4 \text{ Mm}^3$  of material left the source area, and another  $6.6 \text{ Mm}^3$  of material was accumulated from the entrainment area, thus comprising a total volume of  $14 \text{ Mm}^3$ . The simulation results of velocity, maximum velocity, and depth agree with the calculated and observed data. Table 3 shows the comparison of the results obtained from field observations and numerical simulations.

According to the simulation results, the average velocity of the slide was approximately 35 m/s, as shown in Fig. 11. The frame-by-frame analysis of the video footage reveals that the sliding material took 33 s to cover a distance of 1180 m in the valley (35.7 m/s). According to Eq. 5, the slide velocity was 36 m/s, which is approximately equal to the average velocity determined using DAN3D. The maximum velocity of the slide along the runout path was approximately 44 m/s, as indicated by Fig. 12, while Fig. 5 shows the super-elevation and its section along line B-B'. The maximum velocity was recorded at an elevation of approximately 3600 m, just above the point where the slide exits the entrainment area and enters the valley (3300 m). The super-elevation equation yielded a velocity of 42.3 m/s at the same location, thus showing good agreement with the simulated results.

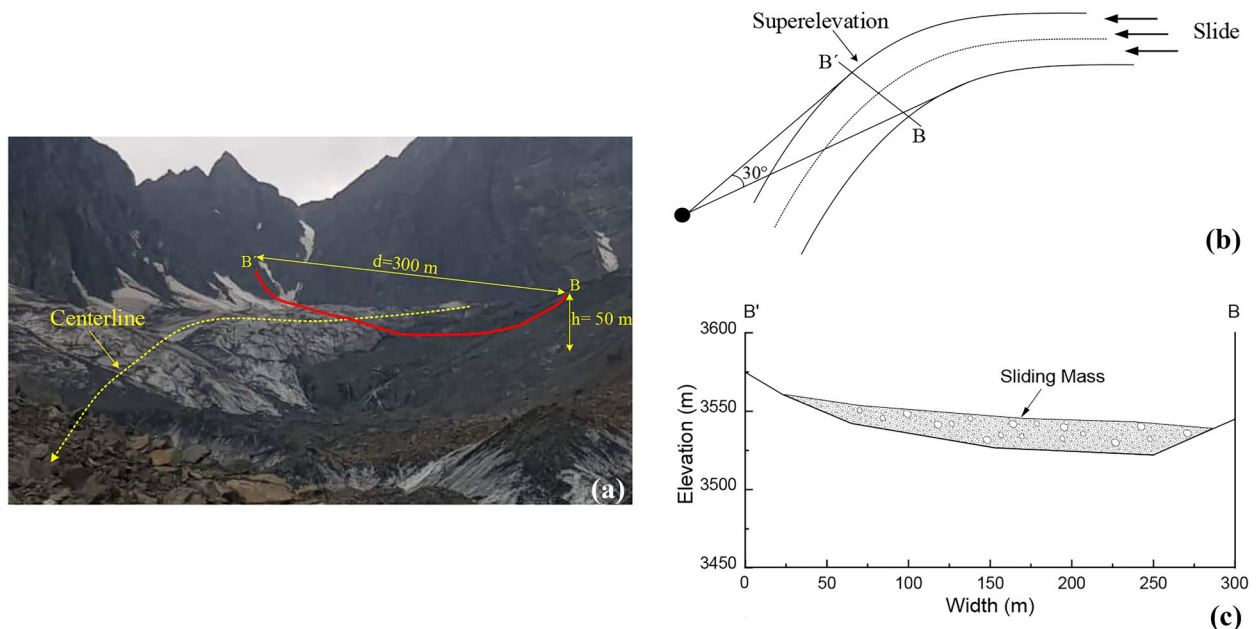


**Fig. 5** Super-elevation along the runout path. (a) The site conditions of the gully (the camera lens faces upstream). (b) The calculation of the super-elevation, where the lens direction is upstream of the gully. (c) Sectional profile along line B-B'

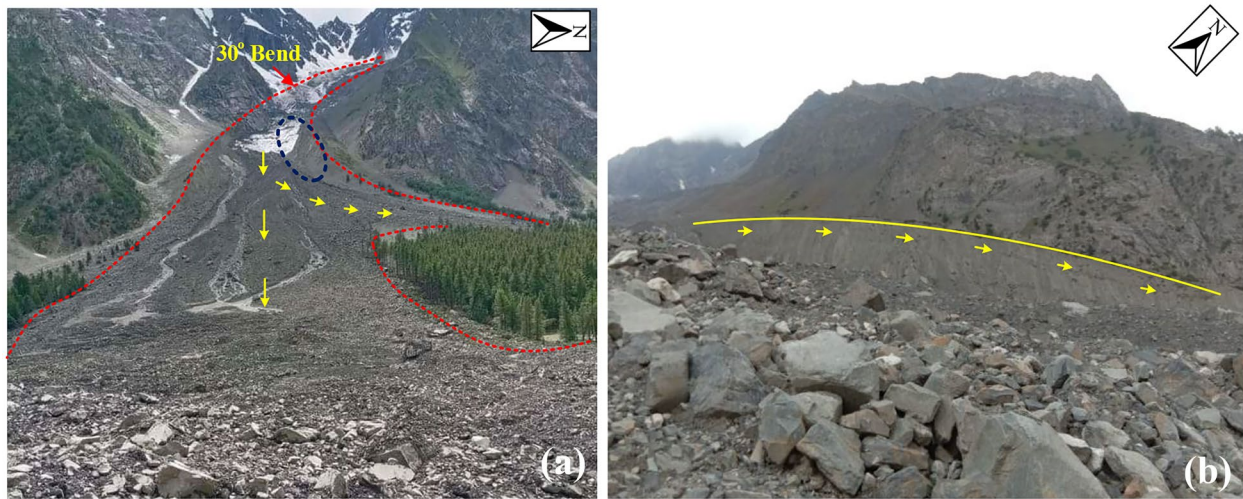


**Fig. 6** Post-landslide images highlighting essential features. **a** shows the two branches of the avalanche, bend in the runout path, and the blue circle marks the location of landslide scarping. **b** Landslide scarp marks

According to field investigation and numerical modeling, the movement process of the upper Naltar valley ice-rock avalanche can be divided into four phases: Phase 1 is from 0 to 20 s, in which the avalanche starts to collapse and accelerates under the action of gravity. Phase 2 is from 20 to 30 s, in which the avalanche enters the entrainment zone and continues its downward motion, as indicated in Fig. 10. Phase 3 is from 90 to 100 s; at an elevation of 3600 m a.s.l., the avalanche turns at an angle of 30°, reaching a maximum velocity near section B-B' Fig. 2a, which was further verified by using Eq. 6 (Zhuang et al. 2020a). Phase 4 is from 100 to 110 s, in which just before entering the valley, the slide divided into two branches: one moved straight, whereas the other diverted at an angle of 54°. The straight branch of the slide moved with an average velocity of 36 m/s, which was verified by video footage. The avalanche came to a complete rest at 140 s, with a maximum deposit depth of approximately 25 m.

Several case studies of high-speed long-runout landslides in North America, South Italy, and China have been conducted using the DAN3D model (Hung and McDougall, 2009; Xing et al. 2014, 2015, 2017; Salvatici et al. 2017; Zhuang et al. 2019; Zhuang et al. 2020a, b; Zhang et al. 2021). In Pakistan, high-speed long-runout landslides are still an undiscovered field; previously, only one study was performed on the famous Attabad 2010 landslide (Gardezi et al. 2021).

The present simulation efficiently reproduced the motion of the upper Naltar valley avalanche and investigated the flow dynamics, thus producing valuable data, as shown in Table 3. The approach adopted in this paper will help to analyze similar kinds of avalanches in the area. Based on a field survey and increased global warming, the author believes that the area is highly prone to high-speed long-runout landslides in the near future. The present case study may be considered the tip of the iceberg in this regard.

**Fig. 7** Effects of the blockage caused by Naltar avalanche. **a** Temporary lake formation resulted due to blockage of the stream flowing through the valley. **b** Dried up creek downstream



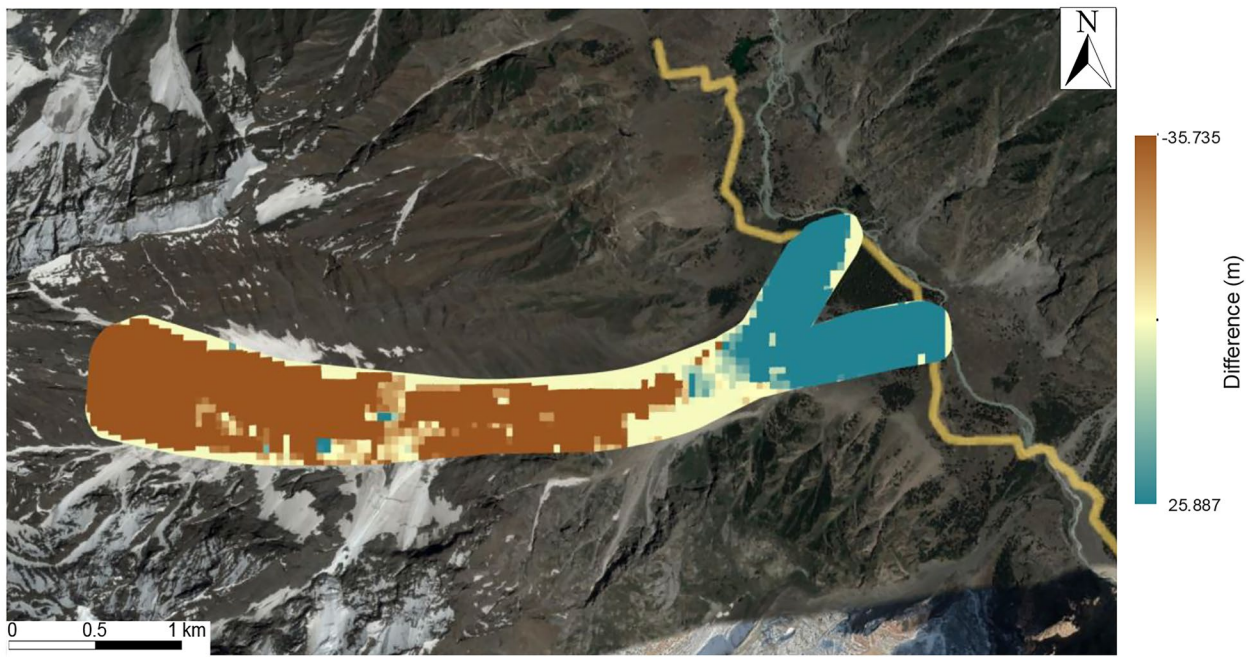
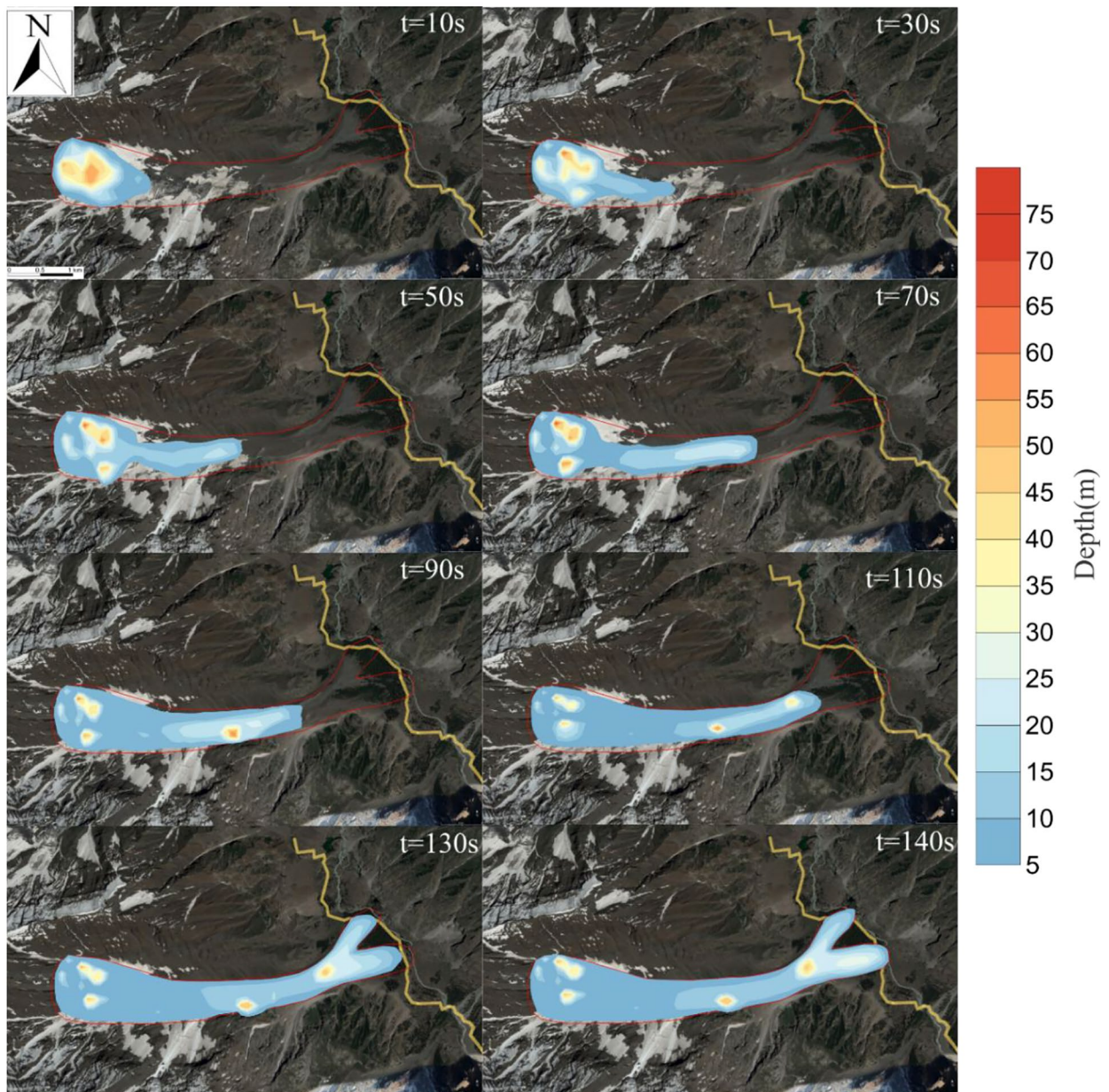


**Fig. 8** Elevation difference before and after the landslide



**Fig. 9** Final depth distribution of the avalanche

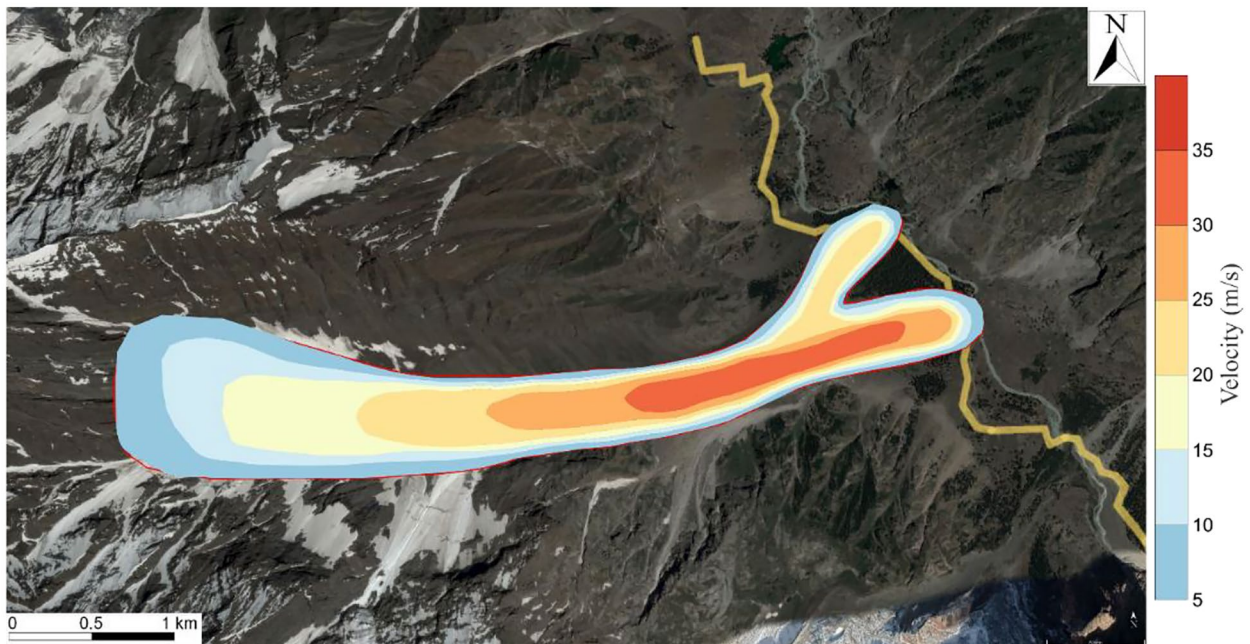




**Fig. 10** Time-lapsed image of deposit depth along the runout path of the avalanche

**Table 3** Simulated and field investigation results comparison

Method	Landslide runout	Runout velocity	Deposit width		Deposit thickness		Landslide duration	
			Straight branch	Left branch	Straight branch	Left branch		
Field investigation	4480 m	-	350 m	300 m	23 m	19 m	-	
Video footage analysis (after entering valley)	1180 m	33 m/s	-	-	-	-	36 s	
Super elevation Eq. (Evans et al. 2001)	-	42.3 m/s	-	-	-	-	-	
Numerical simulation	After landslide enters the valley	1250 m	35 m/s	-	-	-	-	35 s
	Superelevation	-	44 m/s	-	-	-	-	-
	Maximum values (from simulation)	4550 m	45 m/s	362 m	315 m	25	20	140 s

**Fig. 11** Average velocity of the avalanche

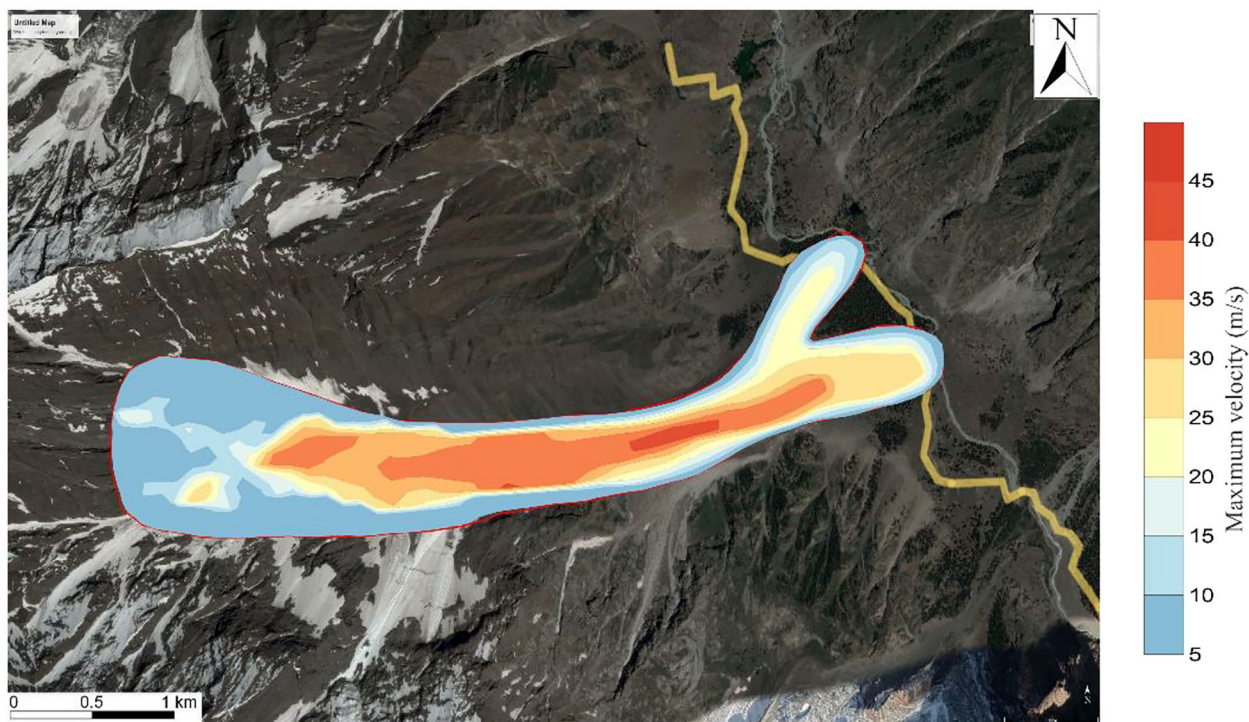


**Fig. 12** Maximum velocity of the avalanche

### Conclusions

On the morning of July 5, 2021, at 09:30 am (PST), a high-speed long-runout ice-rock avalanche hit an area in the upper Naltar valley in the Gilgit district, Pakistan. In this study, we have described the major characteristics of the avalanche based upon field investigations and have studied its runout using the DAN3D model. The conclusions of this study are as follows:

- (1) The upper Naltar valley ice-rock avalanche was a high-speed long-runout landslide that was potentially triggered by the melting of glacial ice caused by global climate change. The avalanche traveled a total distance of 4480 m with an elevation difference of 1830 m and killed four people and hundreds of livestock. It also blocked the stream at two locations, thus forming artificial lakes.
- (2) A three-dimensional dynamic model (DAN3D) was adopted to simulate the runout characteristics of the landslide. The model also accounted for the entrainment of material along the runout path. This study concludes that the DAN3D model produced accurate simulation results, which are consistent with the calculations and field investigations.
- (3) The total duration of the avalanche was estimated to be 140 s, with an average velocity of 32 m/s and a maximum velocity of 42 m/s. The average velocity, maximum velocity, and deposit depth are consistent with the calculations and field investigations, which informs us of the accuracy of selected models and their parameters determined by back calculations.

- (4) This study also concludes that a further temperature increase in summer may cause further events in the area. There are seven massive lakes in the runout paths of potential avalanches; any further sliding activity can cause flooding downstream.
- (5) On the basis of field investigation and numerical modeling, it is recommended that a landslide hazard map of the area along the Naltar expressway be prepared. This was the third incident in the study area in a 1-year time frame, and 2 months after this avalanche, another landslide on the Naltar expressway occurred. Therefore, the immediate need for hazard zoning and preventive measures should be highlighted.

### Acknowledgements

We are thankful to Muhammad Sajjad of National Logistic Cell PMU, Gilgit Baltistan, Site Engineer at Naltar Expressway, for assisting with field investigations.

### Author contribution

Hasnain Gardezi did the simulation work, field investigation work, and wrote the paper; Aiguo Xing designed the research, and helped the revision work; Muhammad Bilal did the field investigation and helped modified the manuscript; Yu Zhuang helped the numerical work and modified the manuscript; Shoaib Muhammad and Shahrir Janjua helped the investigation work.

## Funding

This study was supported by the National Key R&D Program of China (2018YFC1504804) and the National Natural Science Foundation of China (No. 41977215).

## Declarations

**Conflict of interest** The authors declare no competing interests.

## References

- Aaron J, McDougall S, Jordan P (2020) Dynamic analysis of the 2012 Johnsons landing landslide at Kootenay lake, British Columbia: the importance of undrained flow potential. *Can Geotech J* 57:1172–1182. <https://doi.org/10.1139/cgj-2018-0623>
- Abe K, Konagai K (2016) Numerical simulation for runout process of debris flow using depth-averaged material point method. *Soils Found* 56:869–888. <https://doi.org/10.1016/j.sandf.2016.08.011>
- Abraham MT, Satyam N, Kumar S, Reddy P, Pradhan B (2020) Runout modeling and calibration of friction parameters of Kurichemala debris flow. *Landslides, India*. <https://doi.org/10.1007/s10346-020-01540-1>
- Campbell S, Cleary PW, Hopkins M (1995) Large-scale landslide simulations: global deformation, and basal friction. *J Geophys Res* 100:8267–8283
- Chen JX, Ke PZ, Zhang G (2007) Slope stability analysis by strength reduction elasto-plastic FEM. *Key Eng Mater* 345–346:625–628. <https://doi.org/10.4028/www.scientific.net/kem.345-346.625>
- Chen K, Wu J (2018) Simulating the failure process of the Xinmo landslide using discontinuous deformation analysis. *Eng Geol*. <https://doi.org/10.1016/j.enggeo.2018.04.002>
- Chen X, Zhang L, Chen L, Li X, Liu D (2019) Slope stability analysis based on the Coupled Eulerian-Lagrangian finite element method. *Bull Eng Geol Environ* 78:4451–4463. <https://doi.org/10.1007/s10064-018-1413-4>
- Chigira M, Wu X, Inokuchi T, Wang GH (2010) Landslides induced by the 2008 Wenchuan earthquake, Sichuan, China. *Geomorphology* 118: 225–238. <https://doi.org/10.1016/j.geomorph.2010.01.003>
- Crosta GB, Imposimato S, Roddeman DG (2003) Numerical modelling of large landslides stability and runout. *Nat Hazards Earth Syst Sci* 3:523–538. <https://doi.org/10.5194/nhess-3-523-2003>
- Evans SG, Hungr O, Clague JJ (2001) Dynamics of the 1984 rock avalanche and associated distal debris flow on Mount Cayley, British Columbia, Canada; Implications for landslide hazard assessment on dissected volcanoes. *Eng Geol* 61:29–51. [https://doi.org/10.1016/S0013-7952\(00\)00118-6](https://doi.org/10.1016/S0013-7952(00)00118-6)
- Fischer L, Huggel C, Haerberli W (2013) Slope failures and erosion rates on a glacierized high-mountain face under climatic changes. *Earth Surf Process Landforms* 38:836–846. <https://doi.org/10.1002/esp.3355>
- Gardezi H, Bilal M, Cheng Q, Xing A, Zhuang Y, Masood T (2021) A comparative analysis of attabad landslide on January 4, 2010, using two numerical models. *Nat Hazards* 107:519–538. <https://doi.org/10.1007/s11069-021-04593-0>
- Gnyawali KR, Xing A, Zhuang Y (2020) Dynamic analysis of the multi-staged ice-rock debris avalanche in the Langtang valley triggered by the 2015 Gorkha earthquake, Nepal. *Eng. Geol.* 265. <https://doi.org/10.1016/j.enggeo.2019.105440>
- Guerriero L, Revellino P, De Vito A, Grelle G, Guadagno FM (2014) Triggering conditions and runout simulation of the San Mango sul Calore Debris Avalanche, Southern Italy, in: *Advances in Natural and Technological Hazards Research*, pp. 193–204. [https://doi.org/10.1007/978-94-007-7948-8\\_13](https://doi.org/10.1007/978-94-007-7948-8_13)
- Huang Y, Zhang W, Xu Q, Xie P, Hao L (2012) Run-out analysis of flow-like landslides triggered by the Ms 8.0 2008 Wenchuan earthquake using smoothed particle hydrodynamics. *Landslides* 9:275–283. <https://doi.org/10.1007/s10346-011-0285-5>
- Hungr O, Evans SG (2004) Entrainment of debris in rock avalanches: an analysis of a long run-out mechanism. *Bull Geol Soc Am* 116:1240–1252. <https://doi.org/10.1130/B25362.1>
- Hungr O, McDougall S (2009) Two numerical models for landslide dynamic analysis. *Comput Geosci* 35:978–992. <https://doi.org/10.1016/j.cageo.2007.12.003>
- Hutter K, Koch T, Pluüss C, Savage SB (1995) The dynamics of avalanches of granular materials from initiation to runout. Part II Experiments *Acta Mech* 109:127–165. <https://doi.org/10.1007/BF01176820>
- Ishii Y, Ota K, Kuraoka S, Tsunami R (2012) Evaluation of slope stability by finite element method using observed displacement of landslide. *Landslides* 9:335–348. <https://doi.org/10.1007/s10346-011-0303-7>
- Kilburn CRJ, Petley DN (2003) Forecasting giant, catastrophic slope collapse: lessons from Vajont. *Northern Italy* 54:21–32. [https://doi.org/10.1016/S0169-555X\(03\)00052-7](https://doi.org/10.1016/S0169-555X(03)00052-7)
- Kumar R, Nawaz IMBS, Rupendra A (2019) Lake inventory and evolution of glacial lakes in the Nubra - Shyok Basin of Karakoram Range. *Earth Syst. Environ.* <https://doi.org/10.1007/s41748-019-00129-6>
- Leshchinsky B, Vahedifard F, Koo HB, Kim SH (2015) Yumokjeong Landslide: an investigation of progressive failure of a hillslope using the finite element method. *Landslides* 12:997–1005. <https://doi.org/10.1007/s10346-015-0610-5>
- Lin C, Pastor M, Li T, Liu X, Chaoning L, Qi H, Sheng T (2019) A PFE/IE – SPH joint approach to model landslides from initiation to propagation. *Comput Geotech* 114:103153. <https://doi.org/10.1016/j.compgeo.2019.103153>
- Ma Z, Liao H, Dang F, Cheng Y (2021) Seismic slope stability and failure process analysis using explicit finite element method. *Bull Eng Geol Environ* 80:1287–1301. <https://doi.org/10.1007/s10064-020-01989-3>
- McDougall JW, Hussain A, Yeats RS (1993) The Main Boundary Thrust and propagation of deformation into the foreland fold-and-thrust belt in northern Pakistan near the Indus River. *Geol Soc Spec Publ* 74:581–588. <https://doi.org/10.1144/GSL.SP.1993.074.01.38>
- McDougall S, Boulton N, Hungr O, Stead D, Schwab JW (2006) The Zymoetz River landslide, British Columbia, Canada: description and dynamic analysis of a rock slide-debris flow. *Landslides* 3:195–204. <https://doi.org/10.1007/s10346-006-0042-3>
- McDougall S, Hungr O (2004) A model for the analysis of rapid landslide motion across three-dimensional terrain. *Can Geotech J* 41:1084–1097. <https://doi.org/10.1139/T04-052>
- Mergili M, Emmer A, Juřicová A, Cochachin A, Fischer JT, Huggel C, Pudasaini SP (2018) How well can we simulate complex hydro-geomorphic process chains? The 2012 multi-lake outburst flood in the Santa Cruz Valley (Cordillera Blanca, Perú). *Earth Surf Process Landforms* 43:1373–1389. <https://doi.org/10.1002/esp.4318>
- Negi HS, Kanda N, Shekhar MS, Ganju A (2018) Recent wintertime climatic variability over the North West Himalayan cryosphere. *Curr. Sci.* 114. <https://doi.org/10.18520/cs/v114/i04/760-770>
- Pandey P, Ali SN, Champati Ray PK (2021a) Glacier-glacial lake interactions and glacial lake development in the Central Himalaya, India (1994–2017). *J Earth Sci.* <https://doi.org/10.1007/s12583-020-1056-9>
- Pandey P, Chauhan P, Praveen CMB, Suresh KT (2021b) Cause and process mechanism of rockslide triggered flood event in Rishiganga and Dhauliganga River Valleys, Chamoli, Uttarakhand, India using satellite remote sensing and in situ observations. *J Indian Soc Remote Sens* 49:1011–1024. <https://doi.org/10.1007/s12524-021-01360-3>
- Pastor M, Blanc T, Haddad B, Petrone S, Sanchez Morles M, Drempetic V, Issler D, Crosta GB, Cascini L, Sorbino G, Cuomo S (2014) Application of a SPH depth-integrated model to landslide run-out analysis. *Landslides* 11:793–812. <https://doi.org/10.1007/s10346-014-0484-y>
- Pradhan SP, Siddique T (2020) Stability assessment of landslide-prone road cut rock slopes in Himalayan terrain: a finite element method based approach. *J Rock Mech Geotech Eng* 12:59–73. <https://doi.org/10.1016/j.jrmge.2018.12.018>
- Revellino P, Guerriero L, Gerardo G, Hungr O, Fiorillo F, Esposito L, Guadagno FM (2013) Initiation and propagation of the 2005 debris avalanche at nocera inferiore (Southern Italy). *Ital J Geosci* 132:366–379. <https://doi.org/10.3301/IJG.2013.02>

- Runqiu H (2009) Some catastrophic landslides since the twentieth century in the southwest of China. *Landslides* 6: 69–81. <https://doi.org/10.1007/s10346-009-0142-y>
- Salvatici T, Morelli S, Pazzi V, Frodella W, Fanti R (2017) Debris flow hazard assessment by means of numerical simulations: implications for the Rotolon creek valley (Northern Italy). *J Mt Sci* 14:636–648. <https://doi.org/10.1007/s11629-016-4197-7>
- Scheidt C, Rickenmann D, Mcardell BW (2013) Runout Prediction of Debris Flows and Similar Mass Movements 3:221–229. <https://doi.org/10.1007/978-3-642-31310-3>
- Shugar DH, Jacquemart M, Shean D et al (2021) A massive rock and ice avalanche caused the 2021 environmental effects, public safety, and issues associated with justice and rehabilitation disaster at Chamoli, Indian Himalaya tion (19, 20). On 7 February 2021, a massive rock and ice. *Science* (80-. ). 373, 300–306. <https://doi.org/10.1126/science.abh4455>
- Sosio R, Crosta GB, Hungr O (2008) Complete dynamic modeling calibration for the Thurwieser rock avalanche (Italian Central Alps). *Eng Geol* 100:11–26. <https://doi.org/10.1016/j.enggeo.2008.02.012>
- Wang W, Yin K, Chen G, Chai B, Han Z, Zhou J (2019) Practical application of the coupled DDA-SPH method in dynamic modeling for the formation of landslide dam. *Landslides* 16:1021–1032. <https://doi.org/10.1007/s10346-019-01143-5>
- Wu JH, Lin WK, Hu HT (2017) Assessing the impacts of a large slope failure using 3DEC: the Chiu-fen-erh-shan residual slope. *Comput Geotech* 88:32–45. <https://doi.org/10.1016/j.compgeo.2017.03.002>
- Wu Z, Sun J, Chen Y, Wang Q, Zhao W (2015) Analysis of disaster-causing mechanism of loess landslides induced by the Minxian-Zhangxian MS6.6 earthquake, China. 6th Japan-China Geotech. Symp SJGS 2015:40–45. <https://doi.org/10.3208/jgssp.CPN-21>
- Xing A, Wang G, Yin Y, Tang C, Xu Z, Li W (2016) Investigation and dynamic analysis of a catastrophic rock avalanche on September 23, 1991, Zhaotong, China. *Landslides* 13:1035–1047. <https://doi.org/10.1007/s10346-015-0617-y>
- Xing A, Yuan X, Xu Q, Zhao Q, Huang H, Cheng Q (2017) Characteristics and numerical runout modelling of a catastrophic rock avalanche triggered by the Wenchuan earthquake in the Wenjia valley, Mianzhu, Sichuan, China. *Landslides* 14:83–98. <https://doi.org/10.1007/s10346-016-0707-5>
- Xing AG, Wang G, Yin YP, Jiang Y, Wang GZ, Yang SY, Dai DR, Zhu YQ, Dai JA (2014) Dynamic analysis and field investigation of a fluidized landslide in Guanling, Guizhou. *China Eng Geol* 181:1–14. <https://doi.org/10.1016/j.enggeo.2014.07.022>
- Xing AG, Xu Q, Gan JJ (2015) On characteristics and dynamic analysis of the Niujian valley rock avalanche triggered by the 2008 Wenchuan earthquake, Sichuan. *China Environ Earth Sci* 73:3387–3401. <https://doi.org/10.1007/s12665-014-3626-6>
- Xu C, Xu XW, Yao X, Dai FC (2014) Three (nearly) complete inventories of landslides triggered by the May 12, 2008 Wenchuan Mw 7.9 earthquake of China and their spatial distribution statistical analysis. *Landslides* 11: 441–461. <https://doi.org/10.1007/s10346-013-0404-6>
- Yin Y, Xing A, Wang G, Feng Z, Li B, Jiang Y (2017) Experimental and numerical investigations of a catastrophic long-runout landslide in Zhenxiong, Yunnan, southwestern China. *Landslides* 14:649–659. <https://doi.org/10.1007/s10346-016-0729-z>
- Zhang M, Zhou B, Cheng Q, Shen L, Xing A, Zhuang Y (2021) Investigation of the triggering mechanism and runout characteristics of an earthflow in Zhimei village, Chengduo, Qinghai. *China Nat Hazards* 109:903–929. <https://doi.org/10.1007/s11069-021-04861-z>
- Zhang Y, Wang J, Xu Q, Chen G, Zhao X, J, Zheng L, Han Z, Yu P (2015) DDA validation of the mobility of earthquake-induced landslides. *Eng Geol* 194:38–51. <https://doi.org/10.1016/j.enggeo.2014.08.024>
- Zhu C, Huang Y, Zhan L (2018) SPH-based simulation of flow process of a landslide at Hongao landfill in China. *Nat Hazards* 93:1113–1126. <https://doi.org/10.1007/s11069-018-3342-8>
- Zhuang Y, Xing A, Cheng Q, Li D, Zhao C, Xu C (2020a) Characteristics and numerical modeling of a catastrophic loess flow slide triggered by the 2013 Minxian-Zhangxian earthquake in Yongguang village, Minxian, Gansu, China. *Bull Eng Geol Environ* 79:439–449. <https://doi.org/10.1007/s10064-019-01542-x>
- Zhuang Y, Xing A, Cheng Q, Li D, Zhao C, Xu C (2019) Characteristics and numerical modeling of a catastrophic loess flow slide triggered by the 2013 Minxian-Zhangxian earthquake in Yongguang village, Minxian, Gansu, China. *Bull. Eng. Geol. Environ.* <https://doi.org/10.1007/s10064-019-01542-x>
- Zhuang Y, Yin Y, Xing A, Jin K (2020b) Combined numerical investigation of the Yigong rock slide-debris avalanche and subsequent dam-break flood propagation in Tibet, China. *Landslides* 17:2217–2229. <https://doi.org/10.1007/s10346-020-01449-9>

**Hasnain Gardezi · Aiguo Xing (✉) · Muhammad Bilal · Yu Zhuang**

State Key Laboratory of Ocean Engineering, Shanghai Jiao Tong University, Shanghai 200240, China  
Email: xingaiguo@sjtu.edu.cn

**Hasnain Gardezi · Shoaib Muhammad**

Department of Civil Engineering, Wah Engineering College, University of Wah, Wah Cantt 47040, Pakistan

**Shahmir Janjua**

Department of Civil Engineering, Capital University of Science and Technology, Islamabad, Pakistan